J. Fluid Mech. (1973), *vol.* 60, *part* 1, *pp.* 105–127
Printed in Great Britain

Flow past an impulsively started circular cylinder

By W. M. COLLINS AND S. C. R. DENNIS
Department of Applied Mathematics, University of Western Ontario

(Received 10 January 1973)

An accurate method is described for integrating the Navier–Stokes equations numerically for the time-dependent flow past an impulsively started circular cylinder. Results of integrations over the range of Reynolds numbers, based on the diameter of the cylinder, from 5 to ∞ are presented and compared with previous numerical, theoretical and experimental results. In particular, the growth of the length of the separated wake behind the cylinder has been calculated for $R = 40$, 100 and 200 and is found to be in very good agreement with the results of recent experimental measurements. The calculated pressure distribution over the surface of the cylinder for $R = 500$ is also found to be in reasonable agreement with experimental measurements for the case $R = 560$.

For Reynolds numbers up to 100 the equations were integrated until most of the features of the flow showed a close approximation to steady-state conditions. The results obtained are in good agreement with previous calculations of the steady flow past a circular cylinder. For $R > 100$ the integrations were continued until the implicit method of integration broke down by reason of its failure to converge. A secondary vortex appeared on the surface of the cylinder in the case $R = 500$, but for higher Reynolds numbers, including the case $R = \infty$, the procedure broke down before the appearance of a secondary vortex. In all cases the flow was assumed to remain symmetrical.

1. Introduction

Previous theoretical work on the problem of flow past a circular cylinder, which is started impulsively from rest and subsequently moves with constant velocity in a viscous fluid, falls into two main categories. First, the flow for small times after the start may be considered using boundary-layer theory. Blasius (1908), Goldstein & Rosenhead (1936), Schuh (1953), Wundt (1955) and Watson (1955) have all considered this problem in the limiting case of infinite Reynolds number. Wang (1967) and Collins & Dennis (1973) have extended the work to finite but high values of the Reynolds number R. The basis of these applications of unsteady boundary-layer theory is to expand the flow variables in powers of the time from the start of the motion and they are necessarily limited to small times after the start. The results do, however, indicate the basic structure of the initial motion.

The second category is that of purely numerical solutions of the Navier–Stokes equations, and these are on the whole valid for any value of the Reynolds

number. Payne (1958) gave the first numerical solutions for $R = 40$ and 100. Here $R = 2Ua/\nu$, where a is the radius of the cylinder, U is the constant velocity and ν is the coefficient of kinematic viscosity. The Navier–Stokes equations were integrated to moderate values of the time, although the solution at $R = 100$ was still far from the steady state when the integration was terminated. Payne's solutions were reinvestigated by Ingham (1968), who showed that very small time steps must be taken in the integration procedure at the start of the motion to obtain an accurate solution. This is a consequence of the singular nature of the impulsive start. The problem has also been considered by Hirota & Miyakoda (1965), Kawaguti & Jain (1966), Son & Hanratty (1969), Jain & Rao (1969), Thoman & Szewczyk (1969) and Dennis & Staniforth (1971). Kawaguti & Jain considered the Reynolds number range $R = 10$ to 100, while Son & Hanratty gave solutions for $R = 40$, 200 and 500. Thoman & Szewczyk considered the very wide range of $R = 1$ to 10^6. Dennis & Staniforth considered the range $R = 100$ to ∞, but, on the whole, for relatively small times.

One of the major points of interest in the problem is the development of the unsteady separated wake behind the cylinder as a function of time and its structure for large values of the time. In the experiments described by Honji & Taneda (1969) and Taneda (1972), a number of properties of the development of the wake were studied and, in particular, the length of the pair of standing eddies formed behind the cylinder has been measured as a function of time for various values of R. While a comparison of their results for $R = 40$, 100 and 200 with those of existing calculations shows reasonable agreement at small times, some anomalies exist for larger times. For example, there is a substantial difference between the measured wake length of Honji & Taneda (1969) and the calculations of Kawaguti & Jain (1966) at $R = 100$ as the time increases. A similar discrepancy exists, although on a much smaller scale, between the measurements of Honji & Taneda (1969) and the calculations of Son & Hanratty (1969) at $R = 200$. Honji & Taneda (1969) also found that a pair of secondary vortices is formed on the surface of the cylinder at $R = 550$ and above, but not for lower values of R. Secondary vortices were observed by Son & Hanratty (1969) in their calculations at $R = 500$, but they first appear at an earlier time than that estimated by Honji & Taneda (1969) at $R = 550$. Some further investigation of the cases $R = 100$, 200 and 500 would appear to be worthwhile.

One other feature of the time-dependent calculations of both Kawaguti & Jain (1966) and Son & Hanratty (1969) is that, at $R = 40$ (where the calculations can be advanced to an approximate steady state), both solutions agree in obtaining a steady-state wake length considerably greater than that of previously published numerical solutions of the steady-state equations. This case is reinvestigated here by the time-dependent method. It is found that the tendency for large times is more consistent with the steady-state solutions given by Takami & Keller (1969) and Dennis & Chang (1970) than with the tendency of the unsteady solutions cited above, although a comparison of the time-dependent calculations with results of Taneda (1972) tends to be less conclusive in this case. The case $R = 100$ has also been investigated to moderate values of the time in the present paper, in an attempt to obtain some confirmation of the steady-

state solution given by Dennis & Chang (1970). The agreement is found to be satisfactory.

Finally, one of the objects of the present paper is to give a numerical treatment of this problem which is satisfactory both initially, when boundary-layer theory applies, and also at later times, when separation has started and the boundary layer thickens. The methods used, for example, by Payne (1958), Kawaguti & Jain (1966) and Son & Hanratty (1969) do not take into account the initial boundary-layer structure of the flow. These methods are therefore inaccurate initially, and the effect of this inaccuracy on the solution at later times is unknown. The present method of solution employs boundary-layer variables initially. It is to some extent in the spirit of the Galerkin or spectral methods recently discussed by Orszag (1970, 1971). It adopts basically the same type of structure for the solution as that used by Collins & Dennis (1973), except that here the time-dependent integrations are carried out by fully numerical methods rather than by expanding the solutions in series of powers of the time. Thus the initial solution given here may be used to check the solution in powers of the time given by Collins & Dennis (1973). This check is extremely satisfactory. At later times the boundary-layer variables are abandoned, and the solution is continued in the natural space co-ordinates of the problem. The method of integration is an implicit one of Crank–Nicolson type. It is found that, at the higher Reynolds numbers, a time is always reached when this method fails to converge and the integration must be terminated. This breakdown occurs at earlier times as the Reynolds number increases.

2. Basic equations and method of analysis

The same basic formulation of the problem described by Collins & Dennis (1973) is adopted. Modified polar co-ordinates (ξ, θ) are used, where $\xi = \log(r/a)$, a is the radius of the cylinder, and the origin is taken at the centre of the cylinder. The cylinder is suddenly started with velocity U in the direction $\theta = \pi$ and we work in terms of the dimensionless radial and transverse components of velocity (u, v) obtained by dividing the corresponding dimensional components by U. The components (u, v) may be expressed in terms of the dimensionless stream function $\psi(\xi, \theta, t)$ by the equations

$$u = \exp\{-\xi\}(\partial\psi/\partial\theta), \quad v = -\exp\{-\xi\}(\partial\psi/\partial\xi), \tag{1}$$

where ψ satisfies the equation

$$\frac{\partial^2\psi}{\partial\xi^2} + \frac{\partial^2\psi}{\partial\theta^2} = \exp\{2\xi\}\zeta. \tag{2}$$

Here ζ is a dimensionless scalar vorticity function defined by the equation $\zeta = -a\zeta'/U$, where ζ' is the dimensional vorticity. The function ζ satisfies the equation

$$\exp\{2\xi\}\frac{\partial\zeta}{\partial\tau} + \frac{\partial\psi}{\partial\theta}\frac{\partial\zeta}{\partial\xi} - \frac{\partial\psi}{\partial\xi}\frac{\partial\zeta}{\partial\theta} = \frac{2}{R}\left(\frac{\partial^2\zeta}{\partial\xi^2} + \frac{\partial^2\zeta}{\partial\theta^2}\right), \tag{3}$$

where $\tau = Ut/a$ and t is the actual time. The Reynolds number R is defined by $R = 2Ua/\nu$. If the motion starts at $t = 0$, then for all $t > 0$,

$$\psi = \partial\psi/\partial\xi = 0 \quad \text{when} \quad \xi = 0, \tag{4}$$

$$\exp\{-\xi\}(\partial\psi/\partial\theta) \to \cos\theta, \quad \exp\{-\xi\}(\partial\psi/\partial\xi) \to \sin\theta \quad \text{as} \quad \xi \to \infty. \tag{5}$$

In addition, the flow will be assumed to remain symmetrical about the direction of motion of the cylinder. Hence both the functions ψ and ζ are anti-symmetrical about $\theta = 0$ and $\theta = \pi$ and, in particular,

$$\psi = \zeta = 0 \quad \text{when} \quad \theta = 0, \quad \theta = \pi. \tag{6}$$

The method of solution adopted by Collins & Dennis (1973) was to express the functions ψ and ζ in the form of the series

$$\psi = \sum_{n=1}^{\infty} f_n(\xi, \tau)\sin n\theta \tag{7}$$

and

$$\zeta = \sum_{n=1}^{\infty} g_n(\xi, \tau)\sin n\theta, \tag{8}$$

although, in practice, a preliminary transformation of the variable ξ to one more suitable to the initial boundary layer formed on the cylinder was made. The transformation used was

$$\xi = kx, \quad k = 2(2\tau/R)^{\frac{1}{2}}, \tag{9}$$

and thereafter the coefficients of the periodic terms in (7) and (8), when expressed as functions of x and τ, were expanded in series of powers of both τ and k with coefficients which are functions of x. The disadvantage of this approach is that the expansion is limited to relatively small values of τ and k, since only a small number of terms can be calculated, and even then the range of convergence of the series in τ is not known. In the present paper the expansion in powers of τ and k is replaced by a time-dependent method of numerical integration. The integrations are carried out initially using the variable x which is appropriate to the initial boundary layer. The equations are integrated to values of τ well beyond the range of validity of the series expansions in τ and k. Then, at a suitable time after the boundary layer has started to thicken, the variable x is replaced in terms of the original variable ξ and the integration is continued using the equations written in terms of ξ.

The equations necessary for the integrations are found by substituting (7) and (8) into (2) and (3), multiplying each equation by $\sin n\theta$, and integrating with regard to θ from $\theta = 0$ to $\theta = \pi$. Equation (2) becomes

$$\frac{\partial^2 f_n}{\partial\xi^2} - n^2 f_n = \exp\{2\xi\} g_n. \tag{10}$$

Equation (3) can be written as

$$\exp\{2\xi\}\frac{\partial g_n}{\partial\tau} = \frac{2}{R}\frac{\partial^2 g_n}{\partial\xi^2} + nf_{2n}\frac{\partial g_n}{\partial\xi} + \left(\tfrac{1}{2}n\frac{\partial f_{2n}}{\partial\xi} - \frac{2}{R}n^2\right)g_n + S_n, \tag{11}$$

where

$$S_n = \frac{1}{2}\sum_{\substack{m=1 \\ m\neq n}}^{\infty}\left\{[(m+n)f_{m+n} - jf_j]\frac{\partial g_m}{\partial\xi} + m\left[\frac{\partial f_{m+n}}{\partial\xi} - \operatorname{sgn}(m-n)\frac{\partial f_j}{\partial\xi}\right]g_m\right\}.$$

Here $j = |m-n|$ and $\operatorname{sgn}(m-n)$ denotes the sign of $m-n$, with $\operatorname{sgn}(0) = 0$. In both (10) and (11), n can take any positive integer value and the solutions of these two sets of equations define, in theory, two infinite sets of functions $f_n(\xi,\tau)$ and $g_n(\xi,\tau)$. In practice the series (7) and (8) must be truncated by putting identically to zero all terms with subscript $n > n_0$, say, and this defines a truncation of order n_0. All functions with subscripts $n > n_0$ are likewise put zero in (10) and (11), and the $2n_0$ equations (10) and (11) are solved to give an approximation to the flow.

Boundary conditions follow from (4) and (5). From (4) it follows that

$$f_n = \partial f_n/\partial\xi = 0 \quad \text{when} \quad \xi = 0, \tag{12}$$

for all n. As a consequence of the uniform stream condition (5) we must also have that, for all n,

$$g_n(\xi,\tau) \to 0 \quad \text{as} \quad \xi \to \infty. \tag{13}$$

Finally, the condition (5) implies that

$$\exp\{-\xi\} f_n \to \delta_n, \quad \exp\{-\xi\}(\partial f_n/\partial\xi) \to \delta_n \quad \text{as} \quad \xi \to \infty, \tag{14}$$

where

$$\delta_1 = 1, \quad \delta_n = 0 \quad (n = 2, 3, 4, \ldots).$$

If we multiply (10) by $\exp\{-n\xi\}$ and integrate from $\xi = 0$ to $\xi = \infty$, we may deduce, using (12) and (14), that

$$\int_0^\infty \exp\{(2-n)\xi\} g_n(\xi,\tau)\, d\xi = 2\delta_n. \tag{15}$$

Collins & Dennis (1973) showed that the conditions (12), (13) and (15) are sufficient to solve the problem, and that, if they are satisfied and $g_n(\xi,\tau)$ is such that $\exp\{2\xi\} g_n(\xi,\tau)$ is bounded for all n as $\xi \to \infty$, then the flow is automatically adjusted to satisfy the external stream condition (5). The same three conditions are used in the fully numerical solution of the problem.

Equations (10) and (11) determine the development of the flow at some time after the impulsive start, but in the initial stages of the motion the boundary-layer co-ordinate x introduced by the transformation (9) is more appropriate. The functions F_n and G_n defined by the relations

$$f_n = kF_n, \quad g_n = G_n/k \tag{16}$$

are introduced. Equation (10) then becomes

$$\frac{\partial^2 F_n}{\partial x^2} - n^2k^2F_n = \exp\{2kx\} G_n, \tag{17}$$

and equation (11) may be written as

$$4\tau\frac{\partial G_n}{\partial\tau} = \exp\{-2kx\}\frac{\partial^2 G_n}{\partial x^2} + (2x + 4n\tau F_{2n}\exp\{-2kx\})\frac{\partial G_n}{\partial x}$$
$$+\left[2 + \exp\{-2kx\}\left(2n\tau\frac{\partial F_{2n}}{\partial x} - n^2k^2\right)\right] G_n + 4\tau\exp\{-2kx\} S_n^*, \tag{18}$$

where S_n^* is S_n with f_n replaced by F_n, g_n replaced by G_n and ξ replaced by x.

The boundary conditions simply become

$$F_n = \partial F_n/\partial x = 0 \quad \text{when} \quad x = 0, \tag{19}$$

$$G_n(x,\tau) \to 0 \quad \text{as} \quad x \to \infty \tag{20}$$

and

$$\int_0^\infty \exp\{(2-n)\,kx\}\,G_n(x,\tau)\,dx = 2\delta_n. \tag{21}$$

The solution at the start of the motion is found by putting $\tau = 0$ (and hence also $k = 0$) in (17) and (18), and in the condition (21). Equations (18) become

$$\frac{\partial^2 G_n}{\partial x^2} + 2x\frac{\partial G_n}{\partial x} + 2G_n = 0$$

and the only solutions which satisfy (20) and (21) are

$$G_1 = \frac{4}{\pi^{\frac{1}{2}}}\exp\{-x^2\}, \quad G_n = 0 \quad (n = 2, 3, \ldots). \tag{22}$$

The corresponding solutions of (17) (with $k = 0$) satisfying (19) are

$$F_1 = 2\left\{x\,\mathrm{erf}\,x - \frac{1}{\pi^{\frac{1}{2}}}(1-\exp\{-x^2\})\right\}, \quad F_n = 0 \quad (n = 2, 3, \ldots). \tag{23}$$

The initial solution given by (22) and (23) forms the starting point of the solution in powers of τ given by Collins & Dennis (1973), and in the present paper it likewise forms the starting point of the numerical solution of (17) and (18). In the initial stages only a very few terms of the series (7) and (8) are required to describe the flow, but more terms become necessary as the time-dependent integrations proceed. This is exactly analogous to the case of expansion in powers of τ, where each new power of τ introduces higher periodic terms in the expansions (7) and (8). However, the advantage of the present method is that the numerical integrations can be carried on long after the series in powers of τ ceases to be valid, and further the method is not necessarily restricted to high values of R. After the boundary layer thickens it is more realistic to continue the integration in the physical variable ξ, and (10) and (11) are used rather than (17) and (18).

3. Numerical methods

The principle of solving either pair of sets of equations (10) and (11) or (17) and (18) is similar, and is described in detail only for the pair (10) and (11). For a given truncation of order n_0 we must solve $2n_0$ equations, n_0 of type (10) ($n = 1, 2, \ldots, n_0$) and n_0 of type (11). We can write (11) as

$$\frac{\partial g_n}{\partial \tau} = a_n\frac{\partial^2 g_n}{\partial \xi^2} + b_n\frac{\partial g_n}{\partial \xi} + c_n g_n + d_n = q_n(\xi,\tau), \tag{24}$$

where a_n, b_n, c_n and d_n are easily identifiable functions of ξ and τ. The method of solution used is the Crank–Nicolson implicit method, which can be written as

$$g_n(\xi,\tau) - \tfrac{1}{2}Hq_n(\xi,\tau) = g_n(\xi,\tau-H) + \tfrac{1}{2}Hq_n(\xi,\tau-H), \tag{25}$$

where H is the integration step in the τ direction. Central differences are used to approximate the space derivatives in (24), which gives the approximation

$$h^2 q_n(\xi,\tau) = \{a_n(\xi,\tau)+\tfrac{1}{2}hb_n(\xi,\tau)\}g_n(\xi+h,\tau)+\{a_n(\xi,\tau)-\tfrac{1}{2}hb_n(\xi,\tau)\} \times g_n(\xi-h,\tau)+\{h^2c_n(\xi,\tau)-2a_n(\xi,\tau)\}g_n(\xi,\tau)+h^2d_n(\xi,\tau).$$

Substitution of this result in (25) gives

$$\{1+2\gamma a_n(\xi,\tau)-\tfrac{1}{2}Hc_n(\xi,\tau)\}g_n(\xi,\tau)-\gamma\{a_n(\xi,\tau)+\tfrac{1}{2}hb_n(\xi,\tau)\}g_n(\xi+h,\tau) -\gamma\{a_n(\xi,\tau)-\tfrac{1}{2}hb_n(\xi,\tau)\}g_n(\xi-h,\tau) = \tfrac{1}{2}Hd_n(\xi,\tau)+L_n(\xi,\tau-H), \quad (26)$$

where $\gamma = H/2h^2$, h is the grid size in the ξ direction, and $L_n(\xi,\tau-H)$ is the right side of (25) with $q_n(\xi,\tau-H)$ calculated by putting $\tau = \tau-H$ in the expression for $q_n(\xi,\tau)$.

In the step-by-step procedure of integration, the quantity $L_n(\xi,\tau-H)$ is known from the previous time step. Also, $d_n(\xi,\tau)$ on the right side of (26) is independent of the particular function $g_n(\xi,\tau)$ which occurs on the left side. An iterative procedure of solving the set of equations (26) for $n = 1$ to n_0, each equation being an approximate analogue of the corresponding equation (11), may be outlined as follows. The equations are solved in turn from $n = 1$ to n_0. The quantities a_n are independent of n and are known explicitly. The quantities b_n, c_n and d_n are calculated from the most recently available information, using central differences to calculate the derivatives with regard to ξ which appear in the expressions for these quantities. Thus each time an equation of the set (26) is to be solved, the right side may be considered known, and a tri-diagonal matrix of the form

$$A_n(\xi,\tau)g_n(\xi-h,\tau)+B_n(\xi,\tau)g_n(\xi,\tau)+C_n(\xi,\tau)g_n(\xi+h,\tau) = D_n(\xi,\tau), \quad (27)$$

must be solved. The solution is required subject to the conditions (13) and (15). It is obtained in the following manner. A solution $g_n^*(\xi,\tau)$ of the homogeneous set of difference equations obtained by putting $D_n(\xi,\tau) = 0$ in (27) is found to satisfy the conditions $g_n^*(0,\tau) = 1$, $g_n^*(l,\tau) = 0$, where l is some large enough value of ξ. A solution $\tilde{g}_n(\xi,\tau)$ of the full equations (27) is then found to satisfy $\tilde{g}_n(0,\tau) = 1$, $\tilde{g}_n(l,\tau) = 0$. The solution

$$g_n(\xi,\tau) = K_n g_n^*(\xi,\tau)+\tilde{g}_n(\xi,\tau) \quad (28)$$

now satisfies the difference equations (27) and also the condition (13) (in the sense that $\xi = l$ is taken to approximate $\xi \to \infty$) for all values of the constant K_n. The solution (28) is now substituted into the condition (15) and the appropriate integrals are evaluated using numerical integration. The upper limit in each of the integrals is replaced by $\xi = l$, as an approximation. By this procedure the constant K_n can be chosen so that (15) is satisfied; thus (28) then satisfies all the required conditions, or at least approximations to them. The inversion of the tri-diagonal matrices necessary to give $g_n^*(\xi,\tau)$ and $\tilde{g}_n(\xi,\tau)$ was carried out using the method described by Rosser (1967).

After an approximation to the solution of each of the set of equations (11) is obtained by this process, the resulting approximation (28) is used to determine the right side of (10). This equation is then solved by a step-by-step method of

integration subject to the conditions (12). This is a standard problem in theory but a difficult one in practice, because the usual finite-difference methods give extremely unstable formulae of integration when n is large (and here $n_0 = 80$ in some of the cases to be described). A stable and accurate method of integration has been discussed in a report by Dennis & Chang (1969). The method is suitable in the present case provided that l is taken large enough to neglect the integrand in the integral in (15) for $\xi > l$, and so satisfy this condition adequately. Application of the method completes the solution for $f_n(\xi, \tau)$ and $g_n(\xi, \tau)$ for the given value of n, and we then proceed to the next value of n, and so on until $n = n_0$.

The above cycle from $n = 1$ to n_0 is repeated until, ultimately, convergence is achieved. This is decided by the test

$$|g_n^{(m+1)}(\xi, \tau) - g_n^{(m)}(\xi, \tau)| < 10^{-5} \tag{29}$$

for all $n = 1, 2, 3, \ldots, n_0$ and for all grid values of ξ throughout the field, i.e. $\xi = 0, h, 2h, \ldots, l$. Here, the superscripts m, $m+1$ refer to two successive iterates in the cyclic procedure. This iterative procedure converged satisfactorily for small values of τ, but as τ increased it was necessary to introduce the so-called smoothing technique. In this, if we denote the calculated right side of (28) by $\bar{g}_n(\xi, \tau)$, and suppose that the previous iterate for $g_n(\xi, \tau)$ was $g_n^{(m)}(\xi, \tau)$, then the next iterate is defined by the average

$$g_n^{(m+1)}(\xi, \tau) = \kappa \bar{g}_n(\xi, \tau) + (1 - \kappa) g_n^{(m)}(\xi, \tau),$$

where κ is chosen empirically such that $0 < \kappa \leqslant 1$. The case $\kappa = 1$ corresponds to taking the function defined by (28) to be the next iterate. If this process diverges, a reduction of κ will generally secure convergence. As τ increased it was found to be necessary to reduce κ to 10^{-2} to give convergence and, ultimately, it was impossible to achieve convergence at all for the higher values of R, although there appeared to be no problem of convergence for lower values of R.

The method of solution of (17) and (18), which hold when boundary-layer variables are used, is very similar. A typical equation of the set (18) can be written as

$$4\tau \frac{\partial G_n}{\partial \tau} = a_n^* \frac{\partial^2 G_n}{\partial x^2} + b_n^* \frac{\partial G_n}{\partial x} + c_n^* G_n + d_n^* = q_n^*(x, \tau). \tag{30}$$

A slight modification in dealing with (30) is appropriate in view of the fact that it is used near $\tau = 0$. It is better not to divide each side by the factor 4τ to bring it into the form (24) but rather to integrate (30) from $\tau - H$ to τ, integrating the left side by parts, then approximating the resulting integrals by the trapezoidal formula. This gives

$$4(\tau - \tfrac{1}{2}H) G_n(x, \tau) - \tfrac{1}{2}H q_n^*(x, \tau) = 4(\tau - \tfrac{1}{2}H) G_n(x, \tau - H) + \tfrac{1}{2}H q_n^*(x, \tau - H). \tag{31}$$

The reason for this procedure is that the expansion in powers of τ of the function $G_1(x, \tau)$, which dominates the solution at the start of the motion, contains a term of the form $k\phi(x)$. Hence, for any finite value of R, the function $\partial G_1/\partial \tau$ has an algebraic singularity of the form $\tau^{-\frac{1}{2}}$ at $\tau = 0$. Thus, dividing each side of (30) by 4τ and applying the Crank–Nicolson method is unsatisfactory near $\tau = 0$,

and indeed involves an improper integral for the first time step, whereas integration of (30) in the manner indicated smoothes out the effect of the singularity in $\partial G_1/\partial\tau$ at $\tau = 0$. Equation (31), which results from the integration, can now be written as a tri-diagonal matrix by expressing the space derivatives in (30) in terms of grid values in the x co-ordinate by means of three-point central-difference formulae. The numerical solution of this problem in conjunction with a numerical solution of the set of equations (17) is carried out in a similar manner to that already described. The necessary boundary conditions are (19)–(21).

4. Integration procedure

In all cases the integration was started in the boundary-layer variables and the first step is to determine $F_n(x, H)$, $G_n(x, H)$, $(n = 1, 2, \ldots, n_0)$ starting from the initial solution given by (22) and (23). A very small time step H is necessary for this, and in general H must be small throughout the initial stages. The reason is that the expansions of $F_n(x, \tau)$ and $G_n(x, \tau)$ in powers of τ depend also upon integer powers of k (Collins & Dennis 1973), thus all derivatives with respect to τ of terms involving odd powers of k are eventually singular at $\tau = 0$ after a certain stage, provided R is finite. For all finite R the integration was started by taking 10 steps $H = 10^{-4}$ followed by 24 steps $H = 10^{-3}$, which brings the integration to the stage $\tau = 0{\cdot}025$. For high values of R the solution at $\tau = 0{\cdot}025$ checked extremely accurately with the results calculated from the power series in τ given by Collins & Dennis (1973). The series does not converge rapidly enough at low R for the check to be made. Each solution was then continued using a time step $H = 0{\cdot}025$. The grid size in the x co-ordinate was taken to be $h_x = 0{\cdot}050$ in all cases. The quantity l^* taken as the maximum value of x in the field, i.e. the value of x for which the condition $G_n(x, \tau) = 0$ is assumed, was taken as either $l^* = 8$ or $l^* = 10$. This is more than adequate initially, as indicated by the initial solution (22).

As time proceeds the flow separates and the boundary layer thickens and it then becomes unrealistic to continue the integration in boundary-layer variables. The variables are changed to the actual physical variables at some time τ_0. In order that the same grid points shall be used at the time τ_0 for both systems of co-ordinates, the relation $h = 2(2\tau_0/R)^{\frac{1}{2}} h_x$ must hold and τ_0 is therefore chosen so that h, the grid size in the ξ co-ordinate, shall be reasonably small. The integration is then continued in the physical variables until some final time τ_M is reached at which it is terminated. The parameter τ_M depends upon various circumstances which will be described in the following section.

Solutions were carried out for $R = 5$, 10, 40, 100, 200, 500, 1000, 5000 and ∞. The values of the various parameters associated with each case are shown in table 1. The value ξ_M is the value of the field length $\xi = l$ at the time $\tau = \tau_M$ at which the calculations were terminated. This is not necessarily the value of l used at earlier times, but it is the greatest value of l used, for it was found that as the integration proceeded in the physical variables an increasing amount of vorticity was convected further downstream and l had to be increased. The parameter n_0 in table 1 likewise refers to the number of terms of the series (7)

R	τ_M	τ_0	h	ξ_M	n_0
5	15·0	0·30	0·0346	4·85	20
10	20·2	0·60	0·0346	4·85	20
40	30·2	0·80	0·0200	4·40	50
100	25·0	2·00	0·0200	4·40	80
200	13·0	3·55	0·0188	3·39	60
500	4·8	3·20	0·0113	2·50	60
1000	2·0	—	—	—	20
5000	1·5	—	—	—	20
∞	1·25	—	—	—	40

TABLE 1. Parameters used in the numerical solutions

and (8) employed at the final time τ_M. At $\tau = 0$ only one term of each of these series is required, but as the motion continues more terms are gradually required and these are added as they become necessary. The maximum number of terms ($n_0 = 80$) was used in the case $R = 100$. Relatively few terms were used in the cases $R > 500$, because the solutions were taken to relatively small values of τ_M. In these cases, also, the solutions were terminated while the scheme of integration was still in the boundary-layer co-ordinates.

5. Calculated results

The results fall into the three groupings $R < 100$, $R = 100$ and $R > 100$. In the first, it was quite easy to integrate the equations to near to a steady-state solution, although it took a lot of computing time. For $R = 100$, it was possible to integrate until the flow near the cylinder was close to a steady-state solution, but the wake was so slow in developing that the integration procedure had to be terminated ultimately. For $R > 100$ it was impossible to integrate to close to a steady state because a value of τ was always reached at which the implicit integration procedure broke down. This value of τ decreased with increasing R. The termination of the procedure occurs when it fails to converge to the accuracy criterion (29) and, although it may then be possible to obtain convergence for a few further time steps by increasing the right side of (29), such a step must obviously be suspect. Belcher *et al.* (1972) reported that an investigation of the boundary-layer ($R = \infty$) equations by Robins (1970) using the Crank–Nicolson procedure also failed to converge for quite small τ. It is possible that convergence could be improved using techniques described by Israeli (1970, 1972). The procedures used, for example, by Kawaguti & Jain (1966), Son & Hanratty (1969) and Thoman & Szewczyk (1969) are explicit, so that the question of failure of convergence does not arise. The present results in the three groupings mentioned will now be given.

$R < 100$

The solutions at $R = 5$ and $R = 10$ were obtained mainly to check the ability of the method to predict steady-state solutions, and at the same time give some

R	θ_s	L	C_f	C_p	$P(0,\tau)$	$P(\pi,\tau)$
5	—	—	2·01	2·30	−1·08	1·97
10	29·6°	0·52	1·29	1·65	−0·76	1·54
40	53·6°	4·30	0·54	1·02	−0·53	1·16
100	65·4°	7·48	0·30	0·85	−0·54	1·09

TABLE 2. Properties of the solutions for R up to 100 at the final time $\tau = \tau_M$

check on the accuracy at low values of R. Previous solutions obtained by solving the steady-state equations numerically were given at $R = 10$ by Thom (1928), Takami & Keller (1969) and at $R = 5$ and 10 by Dennis & Chang (1970). Kawaguti & Jain (1966) have given a solution of the time-dependent equations for $R = 10$ and the steady-state solution is given as the limit for large time. A solution at $R = 40$ was also given in all of the investigations cited, except that of Thom (1928). In addition, this case has been considered by Kawaguti (1953), who solved the steady-state equations, and by Son & Hanratty (1969), who tackled the time-dependent problem. There is reasonable agreement between all previous investigations at $R = 10$, but some discrepancies exist in the solutions at $R = 40$. The present result at $R = 40$ was taken to a stage closely representing the steady-state solution, although the wake was still expanding slightly when the calculations were terminated.

Estimates of some properties of the solutions at the final values of τ given in table 1 are shown in table 2. The angle θ_s is the separation angle, measured from the rearmost point of the cylinder. Separation starts to occur only for Reynolds numbers greater than about $R = 6$. The values of θ_s in table 2 for $R = 10$ and 40 had certainly approached steady-state values when the integrations were terminated. They are in good agreement with the steady values ($\theta_s = 29{\cdot}6°$ at $R = 10$, $\theta_s = 53{\cdot}8°$ at $R = 40$) given by Dennis & Chang (1970) and also with the values given by Takami & Keller (1969). The quantity $L(\tau)$ is the dimensionless length of the separated wake measured in radii along the axis $\theta = 0$ from the rearmost point of the cylinder to the end of the re-circulating region. The value of L given in table 2 at $R = 10$ is approximately the steady-state value, and is in good agreement with the value $L = 0{\cdot}53$ given by the steady-state solutions of Dennis & Chang (1970). The value $L = 4{\cdot}30$ at $\tau_M = 30{\cdot}2$ for the case $R = 40$ h has not quite settled down to a steady-state value. This is indicated in figure 1, where $L(\tau)$ for $R = 40$ is compared with the experimental points of Honji & Taneda (1972). Estimates of $L(\tau)$ according to the calculations of Kawaguti & Jain (1966) and Son & Hanratty (1969) are also included in figure 1.

Although the length L is obviously still increasing slightly at the termination of the present calculations, the general trend as $\tau \to \infty$ seems to be more consistent with the steady-state value $L = 4{\cdot}69$ given by Dennis & Chang (1970) than with the value of about $L = 5$ given as the limit for large τ by both Kawaguti & Jain (1966) and Son & Hanratty (1969). It is possible that the longer steady-state wake found in both of these latter investigations is due to using a rather coarse grid size $\pi/30$ in the θ direction, as already pointed out by Dennis & Chang (1970).

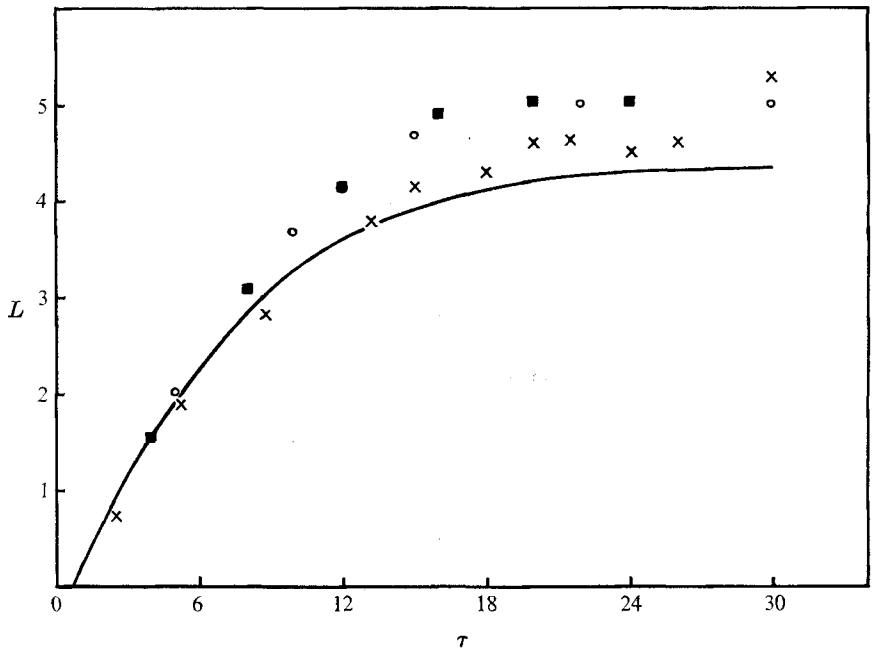

FIGURE 1. Calculated and experimental values for the wake length $L(\tau)$ at $R = 40$. Numerical solutions: ■, Kawaguti & Jain (1966); ○, Son & Hanratty (1969); ——, this study. Experimental measurements: ×, Honji & Taneda (1972).

The experimental results are of little assistance in helping to decide what is the correct theoretical limit for L as $\tau \to \infty$. However a re-calculation of the result of Dennis & Chang (1970) at $R = 40$ using the smaller grid size $\pi/60$ in both ξ and θ directions indicates a slight decrease in the steady-state value of L rather than an increase.

The quantities C_f and C_p in table 2 are the friction and pressure drag coefficients at the final time τ_M. These coefficients together make the total drag coefficient $C_D(\tau)$ defined by $C_D(\tau) = D/\rho U^2 a$ where D is the total drag at any time. It may be shown that

$$C_D(\tau) = \frac{4}{R}\int_0^\pi \left(\zeta - \frac{\partial \zeta}{\partial \xi}\right)_{\xi=0} \sin\theta \, d\theta,$$

where the first term in the integral corresponds to the friction drag coefficient and the second to the pressure drag coefficient. It follows, using (8), (9) and (16), that

$$C_f(\tau) = 2\pi R^{-1} g_1(0,\tau) = \pi(2R\tau)^{-\frac{1}{2}} G_1(0,\tau), \tag{32}$$

$$C_p(\tau) = -2\pi R^{-1}(\partial g_1/\partial \xi)_{\xi=0} = -\pi(4\tau)^{-1}(\partial G_1/\partial x)_{x=0}. \tag{33}$$

At the time of termination of the integrations, the values of $C_f(\tau)$ and $C_p(\tau)$ were still decreasing slightly in all of the cases $R = 5$, 10 and 40. The values in table 2 are, however, all within 5 or 6% of the steady-state values given by Dennis & Chang (1970).

Finally, the values $P(0, \tau_M)$ and $P(\pi, \tau_M)$ in table 2 are the values at $\tau = \tau_M$ and at $\theta = 0$ and $\theta = \pi$, respectively, of the pressure coefficient

$$P(\theta, \tau) = \frac{p(0, \theta, \tau) - p_\infty}{\frac{1}{2}\rho U^2} \tag{34}$$

on the surface of the cylinder. Here $p(\xi, \theta, \tau)$ is the pressure in the fluid and p_∞ is the uniform pressure at large distances from the cylinder. It may be shown that

$$P(\theta, \tau) = P^*(\theta, \tau) + 1 - 2\int_0^\infty \left(\frac{2}{R}\frac{\partial \zeta}{\partial \theta} - \frac{\partial^2 \psi}{\partial \theta\, \partial \tau}\right)_{\theta=\pi} d\xi, \tag{35}$$

where

$$P^*(\theta, \tau) = \frac{4}{R}\int_\theta^\pi \left(\frac{\partial \zeta}{\partial \xi}\right)_{\xi=0} d\theta. \tag{36}$$

This latter coefficient measures the change in dimensionless pressure over the surface of the cylinder starting from the front stagnation point.

The values of $P(\theta, \tau_M)$ at $\theta = 0$ and π for $R < 100$ in table 2 are all within 5 % of the final steady-state values given by Dennis & Chang (1970). At the final time $\tau = \tau_M$ the coefficient $P(\theta, \tau)$ is still changing slowly in the direction of the steady-state results over the whole surface of the cylinder for each value of R, but the results are quite close to the steady-state results of Dennis & Chang (1970). There can therefore hardly be any doubt that, for the range of R up to 40, the method of integration gives solutions which approach a steady state. In all cases the integrations could have been continued to larger times.

$R = 100$

This case is one of the most interesting. The growth of the wake length $L(\tau)$ with τ is shown in figure 2, where it is compared with the experimental points of Honji & Taneda (1972). The agreement is seen to be excellent in this case. The results of the calculations performed by Kawaguti & Jain (1966) are also shown; the departure of these from the experimental measurements is almost certainly due to inaccurate calculation, for Kawaguti & Jain use the same grid size $\pi/30$ in the θ direction which they use for $R = 40$, and this is thought to be inadequate even in this latter case. The development of the vorticity on the surface of the cylinder with τ is shown in figure 3. It will be seen that the distribution of vorticity over the surface remains smooth up to $\tau = 2$, but that at some time thereafter the curves develop a kink in the separated region $0 < \theta < \theta_s$. This kink continues to be present as τ increases, although it never becomes sufficiently pronounced (as it does for higher values of R) for the vorticity to change sign within the separated region, which would imply the existence of a secondary vortex. Moreover, as τ increases further, the kink eventually becomes less pronounced, until for $\tau = 20$ it has more or less completely vanished. After this, the curves appear to approach the steady-state solution given by Dennis & Chang (1970). A comparison between this solution and the situation reached at $\tau = 25$ is given in figure 4. The agreement is extremely satisfactory, bearing in mind that the region around the maximum vorticity ($\theta \approx 135°$) is always the last region on the surface to settle down to the steady-state solution, and that it had not completely settled down at this time.

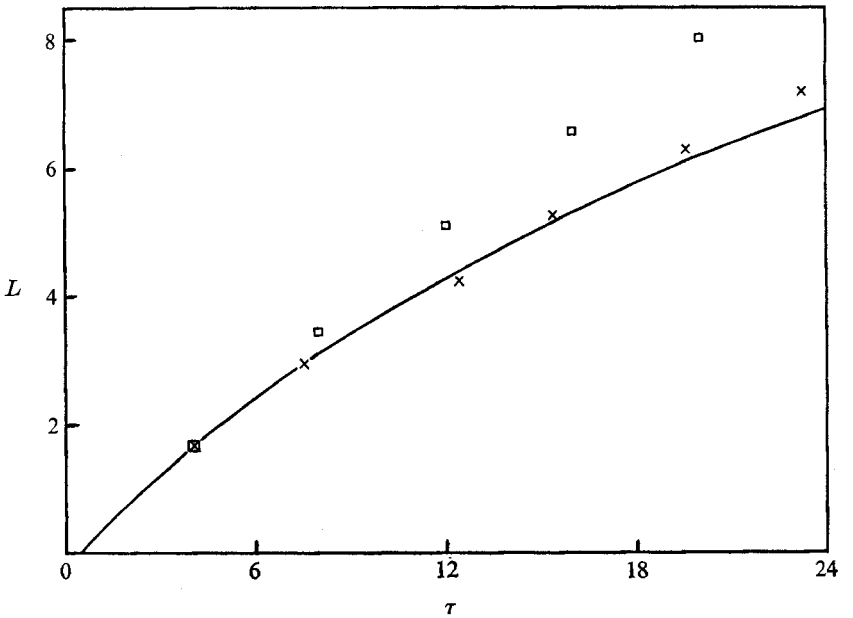

FIGURE 2. Calculated and experimental values for the wake length $L(\tau)$ at $R = 100$. Numerical solutions: □, Kawaguti & Jain (1966); ——, this study. Experimental measurements: ×, Honji & Taneda (1972).

The values of the drag coefficients $C_f(\tau)$ and $C_p(\tau)$ at $\tau = 25$ given in table 2 for $R = 100$ are a little higher than the steady-state values ($C_f(\infty) = 0{\cdot}282$, $C_p(\infty) = 0{\cdot}774$) given by Dennis & Chang (1970). This is quite consistent with the comparison of figure 4. The wake length $L(\tau)$ at $\tau = 25$ is only just over half the steady-state value (13·1) reported by Dennis & Chang (1970), but this is again consistent with the fact that the integrations take a long time to settle in the wake region. Finally, the solution procedure was terminated at $\tau = 25$, because the iterative procedure failed to converge to an acceptable criterion of accuracy. Although it may be possible to continue the integration using an explicit method, the failure of the implicit method was taken as an indication that the solution was becoming unstable. It may be noted that, in the case $R = 100$, the time $\tau = 25$ is quite consistent with the time at which Honji & Taneda (1969) noticed instability in the wake with an eventual transition to a turbulent wake.

$R > 100$

The solutions for $R > 100$ are all characterized by the fact that the integrations could be carried out only for a relatively short time before the procedure broke down and that the time τ_M decreased as R increased. In figure 5 the growth of wake length $L(\tau)$ is shown in comparison with the results of Honji & Taneda (1972) and the calculated results of Son & Hanratty (1969) for the case $R = 200$. The wake length given by Son & Hanratty generally seems to be greater than that of the present calculations, at the same value of τ. This could be because Son & Hanratty give separation as first occurring at $\tau_s = 0{\cdot}36$, whereas the present

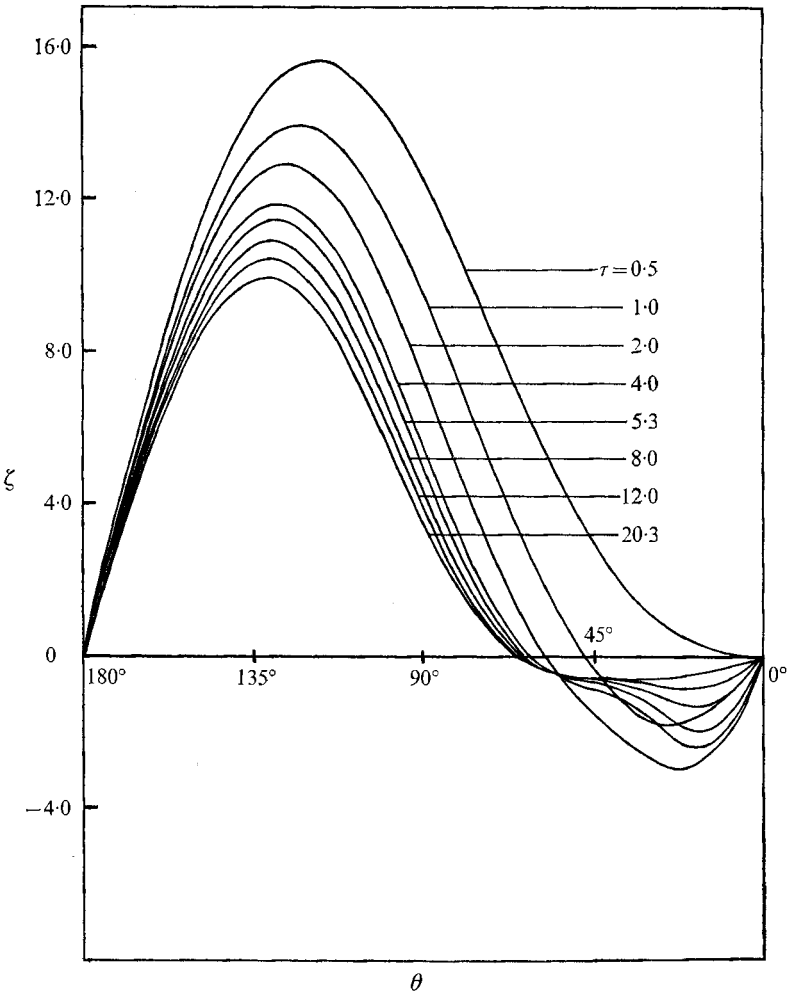

FIGURE 3. Vorticity distribution over the surface of the cylinder for $R = 100$.

R	100	200	500	1000	5000	∞
Series	0·589	0·458	0·396	0·371	0·343	0·322
Present	0·513	0·445	0·394	0·371	0·343	0·322

TABLE 3. Comparison of the separation time τ_s between the series method of Collins & Dennis (1973) and the present results

investigation gives it considerably later at $\tau_s = 0{\cdot}445$. The present result is in good agreement with the value $\tau_s = 0{\cdot}458$ obtained from the series in powers of τ given by Collins & Dennis (1973), and a general comparison between the values of τ_s given by the two methods is shown to be somewhat as might be expected in table 3.

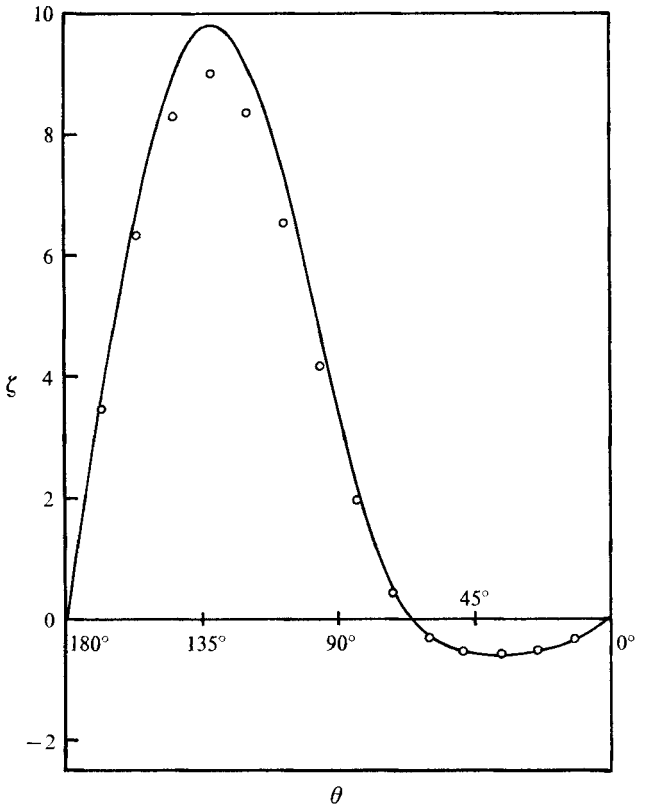

FIGURE 4. Comparison of the vorticity distribution over the surface of the cylinder at $R = 100$: ——, present solution at $\tau = 25$; ○, steady-state solution of Dennis & Chang (1970).

In figure 6, the variation of the angle of separation with τ is shown for the whole range of R considered. Although the integrations for the higher values of R had to be terminated at relatively small values of τ, the trend of the results is consistent with the work of Son & Hanratty (1969) and Thoman & Szewczyk (1969), particularly in that, for high R, θ_s appears to tend to values considerably in excess of those predicted by steady boundary-layer theory with external potential flow. Also, the tendency of θ_s for $R = \infty$ agrees extremely well with the estimates from the series in powers of τ obtained by Collins & Dennis (1973) up to $\tau = 1$, and even at $\tau = 1$ the difference between the two estimates is less than 0·5 %. Indeed, virtually all the properties of the $R = \infty$ solution given by Collins & Dennis (1973) have been checked to this order of accuracy up to $\tau = 1$, which gives some theoretical check on the present method.

One of the reasons for finding a solution at $R = 500$ was to attempt to check the calculations of Son & Hanratty (1969). The experiments of Honji & Taneda (1969) indicate that at $R = 550$ a pair of secondary vortices are formed on the surface of the cylinder, first making their appearance at about $\tau = 4{\cdot}98$. Secondary vortices were also observed for flows for which $R > 550$, but none were observed in flows for Reynolds numbers below 550. The calculations of Son & Hanratty

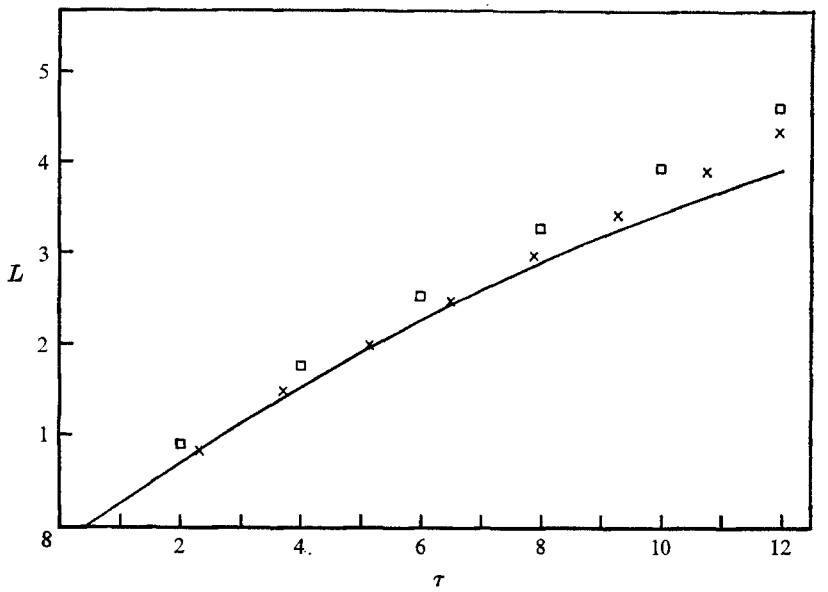

FIGURE 5. Calculated and experimental values for the wake length $L(\tau)$ at $R = 200$. Numerical solutions: □, Son & Hanratty (1969); ——, this study. Experimental measurements: ×, Honji & Taneda (1972).

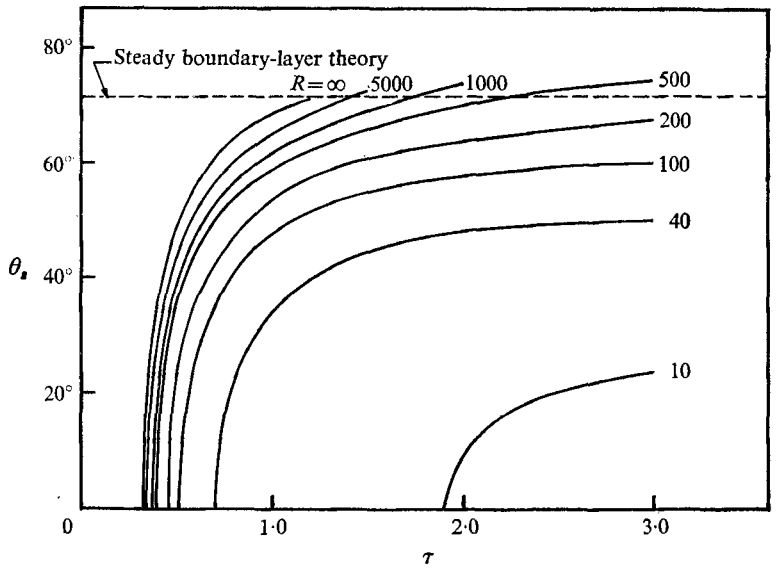

FIGURE 6. Variation of the angle of separation θ_s with τ.

(1969) at $R = 500$ also indicate the appearance of a pair of secondary vortices. They first appear at about $\tau = 2{\cdot}78$, which is much smaller than the corresponding value of τ for the experiments at $R = 550$, and eventually decrease in size and disappear completely at $\tau = 56$. The present results confirm these calculations for the early stages of the flow in that the secondary vortices first make their

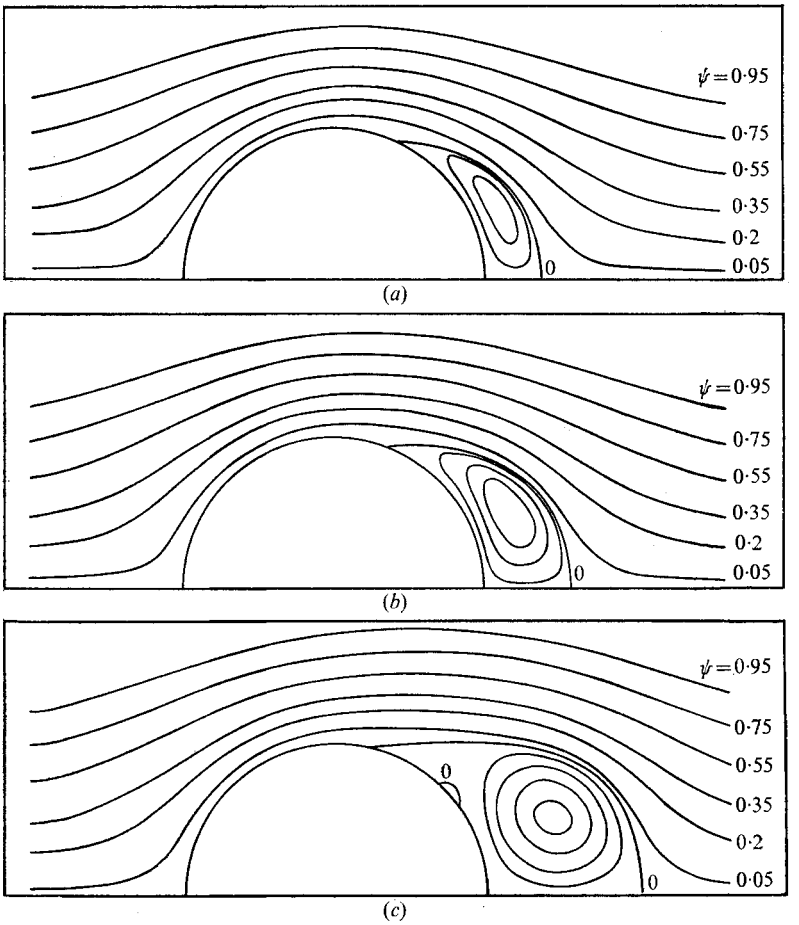

FIGURE 7. Development of the streamlines with time at $R = 500$ for (*a*) $\tau = 1{\cdot}5$, (*b*) $\tau = 2{\cdot}0$, (*c*) $\tau = 3{\cdot}2$.

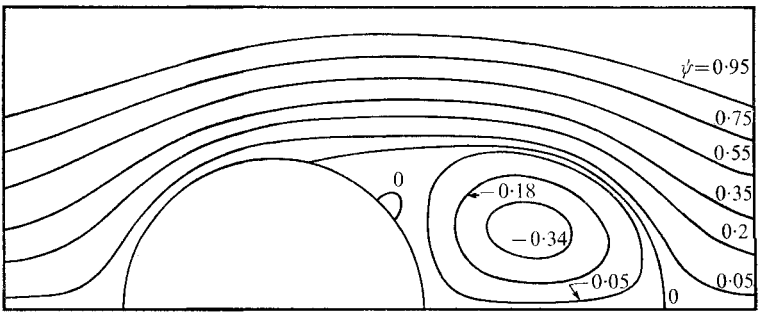

FIGURE 8. Streamlines at $R = 500$ for the final time $\tau_M = 4{\cdot}8$.

appearance at about $\tau = 2{\cdot}75$, but the calculations could only be continued until $\tau = 4{\cdot}8$, at which stage the procedure broke down.

The development of the flow patterns with time until shortly after the onset of the secondary vortices is shown in figure 7, and the streamline pattern at the final time $\tau_M = 4{\cdot}8$ is given in figure 8. The flow pattern in figure 8 compares quite

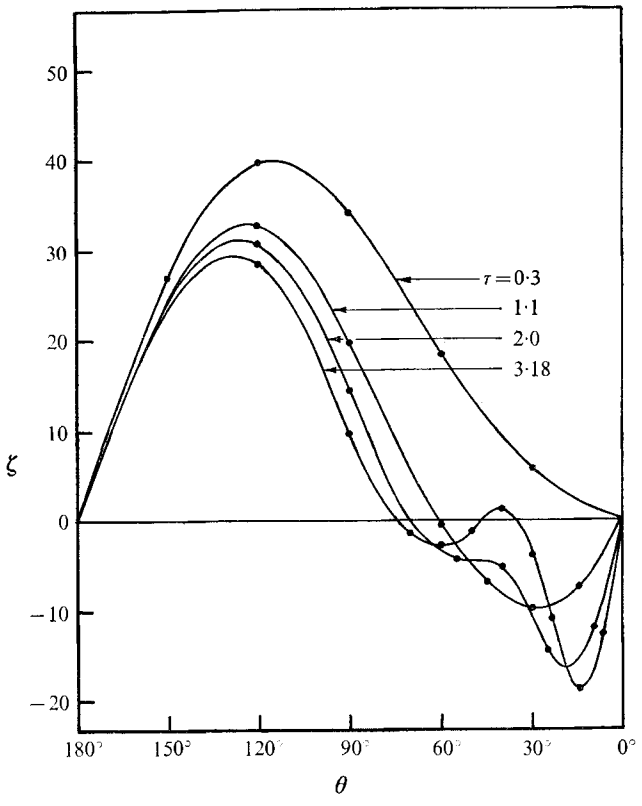

FIGURE 9. Comparison of the vorticity distribution over the surface of the cylinder at $R = 200$; ●, Son & Hanratty (1969); ——, present study.

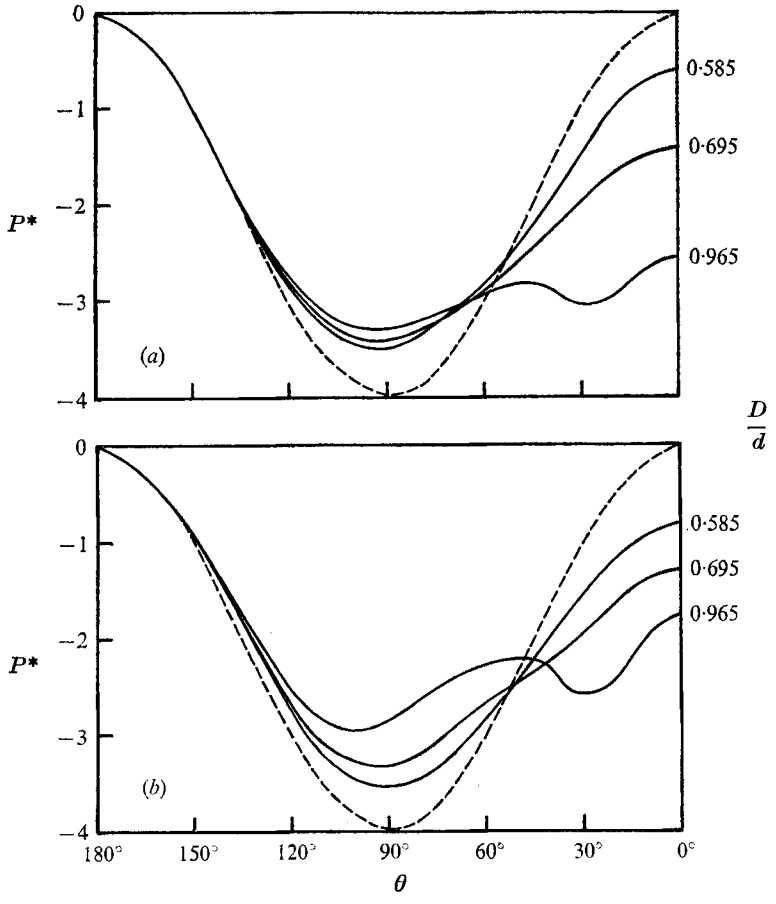

FIGURE 10. Variation of the pressure coefficient $P^*(\theta, \tau)$ over the surface of the cylinder for (*a*) the experimental measurements of Schwabe (1935) at $R = 560$, (*b*) the present calculations at $R = 500$. The dotted curves correspond to potential flow.

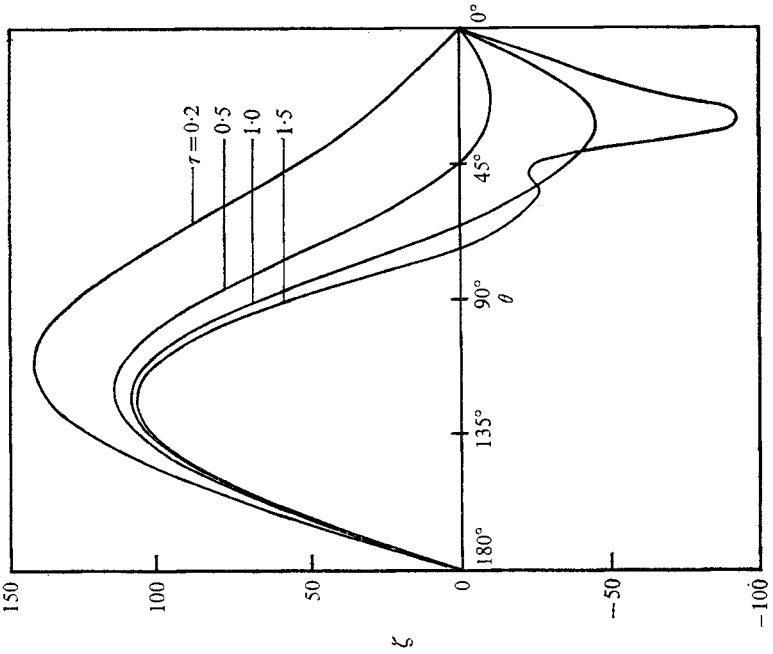

FIGURE 12. Vorticity distribution over the surface of the cylinder for $R = 5000$.

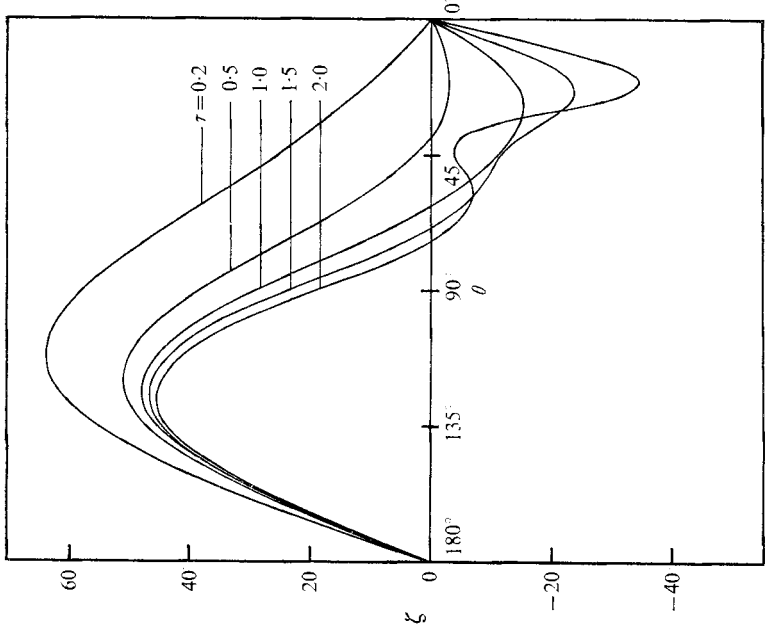

FIGURE 11. Vorticity distribution over the surface of the cylinder for $R = 1000$.

favourably with the photograph at $\tau = 4{\cdot}98$ for $R = 550$ in Honji & Taneda (1969, figure 14, p. 1673). There is also an excellent comparison with the results of Son & Hanratty (1969), and this is shown for one property (surface vorticity) in figure 9. In figure 10 the pressure variation around the cylinder surface according to the present calculation at $R = 500$ is compared with the experimental measurements of Schwabe (1935) for the case $R = 560$. The pressure coefficient $P^*(\theta, \tau)$ defined by (36) is used for this comparison. Schwabe (1935) gives curves at times corresponding to various values of D/d, where D is the distance from the centre of the cylinder to the end of the separated region and d is the diameter of the cylinder. The same values of D/d are used as a basis for comparison of the present results. On the whole, the comparison seems satisfactory.

The solutions for $R = 1000$ and 5000 do not add greatly to the knowledge of the problem, except to confirm certain general tendencies. The development of surface vorticity with time is shown for these cases in figures 11 and 12 respectively. These diagrams indicate that the distortion of vorticity in the separated region $0 < \theta < \theta_s$ occurs at an earlier value of τ as R increases. However, the integration procedure failed in each case before a secondary vortex was formed. This is hardly surprising, in view of the relatively large amount of vorticity produced in the region of reversed flow immediately prior to the failure. This is well illustrated in figure 12, where the magnitude of the greatest surface vorticity produced in the region $0 < \theta < \theta_s$ at the final value $\tau_M = 1{\cdot}5$ is almost equal to the magnitude of the maximum vorticity in the unseparated region. Because of the failure of the present procedure at increasingly small values of τ as R increases, it is felt that some caution should be exercised in evaluating the solutions given for large R and τ by Thoman & Szewczyk (1969), and even by Son & Hanratty (1969), for large τ at $R = 200$ and 500. The experimental results of Honji & Taneda (1969, figure 7, p. 1671) indicate that a transition from a laminar to a turbulent wake takes place at values of τ that we estimate† to be about $\tau = 24$, 16, 11 and 8 at the values $R = 100$, 200, 500 and 1000, respectively. The laminar equations would not be expected to apply for values of τ greater than these critical values. It could also be conjectured that there is some qualitative correlation between these critical values of τ, and the values of τ_M in table 1 at which the calculations broke down.

A similar breakdown of the procedure was found to occur in the case $R = \infty$. Here the integration could not be continued beyond $\tau = 1{\cdot}25$. Two attempts at integrating the unsteady boundary-layer equations by finite-difference methods in this case have been described by Belcher *et al.* (1972). In the first, the Crank–Nicolson procedure was used, and it was found that the method had to be abandoned at $\tau = 0{\cdot}45$. A more elaborate implicit method succeeded in carrying the integration to $\tau = 2$, although inaccuracies appeared near the separation point at $\tau = 1$, and spread in both directions of θ. The situation therefore appears to be very similar to that experienced in the present integration. Very similar results were also found in this case by Dennis & Staniforth (1971), who applied

† The estimation is made from the graph cited. The symbol τ in the present paper is $2R$ times the corresponding symbol used by Honji & Taneda (1969).

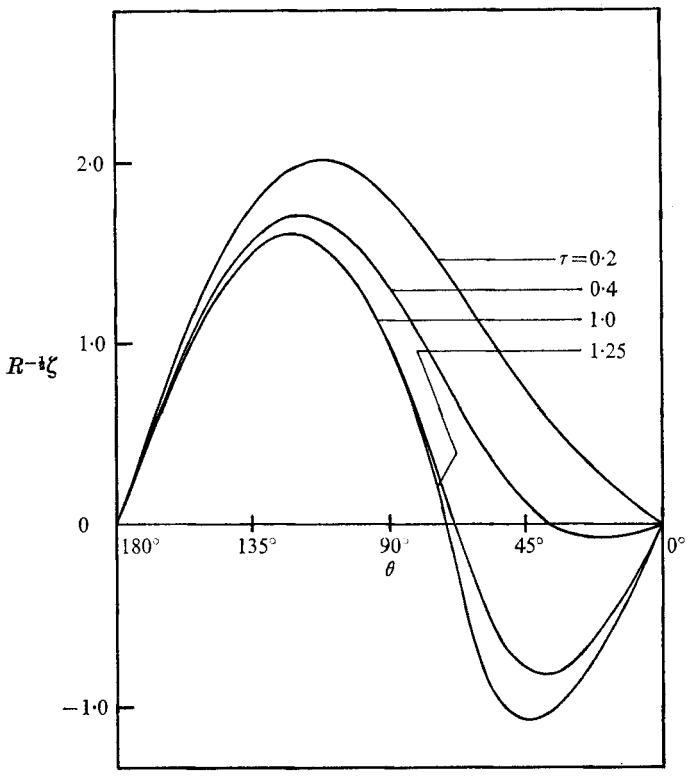

FIGURE 13. Distribution of $R^{-\frac{1}{2}}\zeta$ over the surface of the cylinder for $R = \infty$.

a two-dimensional finite-difference method of Crank–Nicolson type to the equation obtained by expressing the basic equation (3) in terms of boundary-layer variables. Solutions using this method were also given by Dennis & Staniforth (1971) for $R = 100$, 500, 1000 and 10^4 but, on the whole, covering smaller ranges of τ than those of the present paper. Difficulties with regard to convergence of the procedure were encountered at the higher Reynolds numbers.

In figure 13 the quantity $R^{-\frac{1}{2}}\zeta(0, \theta, \tau)$ is given as a function of the angle θ for various values of τ for the case $R = \infty$. This is a measure of $R^{\frac{1}{2}}$ times the local dimensionless coefficient of skin friction on the surface of the cylinder. The agreement with the results obtained from the series in powers of τ given by Collins & Dennis (1973) is excellent up to $\tau = 1$. There is also good agreement with the results of Belcher *et al.* (1972). All investigations appear to agree reasonably well with the prediction of Proudman & Johnson (1962) that the slope of the local skin friction curve at $\theta = 0$ should tend to the same value as the slope at $\theta = \pi$ as τ becomes large. Various other properties of the $R = \infty$ solution were calculated, and are found to be in good agreement for values of τ up to $\tau = 1$ with the results of Collins & Dennis (1973). No secondary vortex was found to occur up to the time $\tau_M = 1{\cdot}25$ at which the calculations terminated.

A detailed account of the numerical method used for solving the set of differential equations (10) is given in Dennis & Chang (1969). Copies of this report

can be obtained from the Mathematics Research Center, University of Wisconsin, Madison, Wisconsin. A copy has also been deposited in the editorial office of the Journal of Fluid Mechanics.

The work was supported by grants from the National Research Council of Canada. The calculations were carried out on the IBM 7040 and CDC 6400 computers of the University of Western Ontario, and on the CDC 6600 computer of the General Computer Corporation of Toronto.

REFERENCES

BELCHER, R. J., BURGGRAF, O. R., COOKE, J. C., ROBINS, A. J. & STEWARTSON, K. 1972 *Recent Research on Unsteady Boundary Layers*, vol. 2 (ed. E. A. Eichelbrenner). Quebec: Laval University Press.

BLASIUS, H. 1908 *Z. Math. Phys.* **56**, 1.

COLLINS, W. M. & DENNIS, S. C. R. 1973 *Quart. J. Mech. Appl. Math.* **26**, 53.

DENNIS, S. C. R. & CHANG, G. Z. 1969 *Math. Res. Center, University of Wisconsin, Tech. Summary* Rep. 859.

DENNIS, S. C. R. & CHANG, G. Z. 1970 *J. Fluid Mech.* **42**, 471.

DENNIS, S. C. R. & STANIFORTH, A. N. 1971 *Lecture Notes in Physics* **8**, 343.

GOLDSTEIN, S. & ROSENHEAD, L. 1936 *Proc. Camb. Phil. Soc.* **32**, 392.

HIROTA, I. & MIYAKODA, K. 1965 *J. Met. Soc. Japan, Ser.* II, **43**, 30.

HONJI, H. & TANEDA, S. 1969 *J. Phys. Soc. Japan*, **27**, 1668.

HONJI, H. & TANEDA, S. 1972 *Rep. Res. Inst. Appl. Mech. Kyushu University*, **19**, 265.

INGHAM, D. B. 1968 *J. Fluid Mech.* **31**, 815.

ISRAELI, M. 1970 *Studies in Appl. Math.* **49**, 327.

ISRAELI, M. 1972 *Studies in Appl. Math.* **51**, 67.

JAIN, P. C. & RAO, K. S. 1969 *Phys. Fluids Suppl.* II, **12**, II-57.

KAWAGUTI, M. 1953 *J. Phys. Soc. Japan*, **8**, 747.

KAWAGUTI, M. & JAIN, P. C. 1966 *J. Phys. Soc. Japan*, **21**, 2055.

ORSZAG, S. A. 1970 *J. Atmos. Sci.* **27**, 890.

ORSZAG, S. A. 1971 *Studies in Appl. Math.* **50**, 293.

PAYNE, R. B. 1958 *J. Fluid Mech.* **4**, 81.

PROUDMAN, I. & JOHNSON, K. 1962 *J. Fluid Mech.* **12**, 161.

ROBINS, A. J. 1970 Ph.D. thesis, University of Bristol.

ROSSER, J. B. 1967 *Math. Res. Center, University of Wisconsin, Tech. Summary* Rep. 797.

SCHUH, H. 1953 *Z. Flugwis.* **1**, 122.

SCHWABE, M. 1935 *Ing.-Arch.* **6**, 34.

SON, J. S. & HANRATTY, T. J. 1969 *J. Fluid Mech.* **35**, 369.

TAKAMI, H. & KELLER, H. B. 1969 *Phys. Fluids Suppl.* II, **12**, II-51.

TANEDA, S. 1972 *Recent Research on Unsteady Boundary Layers*, vol. 2 (ed. E. A. Eichelbrenner). Quebec: Laval University Press.

THOM, A. 1928 *Aero. Res. Counc. R. & M.* no. 1194.

THOMAN, D. C. & SZEWCZYK, A. A. 1969 *Phys. Fluids Suppl.* II, **12**, II-76.

WANG, C. Y. 1967 *J. Math. Phys.* **46**, 195.

WATSON, E. J. 1955 *Proc. Roy. Soc.* A **231**, 104.

WUNDT, H. 1955 *Ing.-Arch.* **23**, 212.